

Nanoscale Chemical Imaging of Single-Layer Graphene

Johannes Stadler, Thomas Schmid, and Renato Zenobi*

Department of Chemistry and Applied Biosciences, ETH Zurich, CH-8093 Zurich, Switzerland

Since the discovery of buckminsterfullerene in 1985,¹ a growing interest in carbon modifications yielded a variety of carbon allotropes with special shapes and properties, such as single- and multiwalled carbon nanotubes, “bucky balls”, lonsdaleite, carbon nanobuds and nanofibres, graphene whiskers, graphene ribbons, and multi- and single-layer graphene (SLG). After the discovery of graphene in 2004,² Novoselov *et al.* demonstrated a simple production method called the scotch-tape technique³ that made graphene easily available to researchers around the world. Graphene is nowadays not only subject to intense basic research but also made its way into different applications such as printed circuits,⁴ transistors for frequencies up to the GHz range,^{5,6} supercapacitors,⁷ or ultrafast photodetectors.⁸ Electronic devices are usually produced either from SLG produced by the scotch-tape technique and deposited on SiO₂/Si for identification with consecutive top-gating or from graphene films that are first produced by CVD on Cu films⁹ and then transferred onto other substrates by dissolving the Cu support layer and transferring the graphene film using a PMMA layer.¹⁰ The electronic properties of these graphene-based devices strongly depend on a correctly designed graphene sheet. Lattice defects at the ribbon edges are expected to contribute to Anderson localization,¹¹ and disorder within the sheet or nanoribbon of graphene can, for example, influence the band gap; charged impurities and ripples are relevant when the mobility of electrons is of importance for the manufactured device.⁵ Furthermore, selective placement of extended defects can strongly enhance conductivity of graphene nanoribbons,¹² enabling them to process information or carry spin polarizing current,¹³ making a localization of defects compulsory for characterization.

Several analytical techniques such as electron microscopy (EM), scanning tunneling microscopy (STM), or atomic force microscopy

ABSTRACT Electronic properties in different graphene materials are influenced by the presence of defects and their relative position with respect to the edges. Their localization is crucial for the reliable development of graphene-based electronic devices. Graphene samples produced by standard CVD on copper and by the scotch-tape method on gold were investigated using tip-enhanced Raman spectroscopy (TERS). A resolution of <12 nm is reached using TERS imaging with full spectral information in every pixel. TERS is shown to be capable of identifying defects, contaminants, and pristine graphene due to their different spectroscopic signatures, and of performing chemical imaging. TERS allows the detection of smaller defects than visible by confocal Raman microscopy and a far more precise localization. Consecutive scans on the same sample area show the reproducibility of the measurements, as well as the ability to zoom in from an overview scan onto specific sample features. TERS images can be acquired in as few as 5 min with 32 × 32 pixels. Compared to confocal Raman microscopy, a high sensitivity for defects, edges, hydrogen-terminated areas or contaminated areas (in general for deviations from the two-dimensional structure of pristine graphene) is obtained due to selective enhancement as a consequence of the orientation in the electromagnetic field.

KEYWORDS: single-layer graphene · tip-enhanced Raman spectroscopy · confocal Raman microscopy

(AFM) as well as Raman spectroscopy (RS) have been used to study the properties of graphene and image its structure.^{14–20} Due to the clear and pronounced vibrational spectra of graphene, Raman spectroscopy is ideally suited to investigate graphene²¹ and delivers information about the number of layers,^{22,23} strain,^{24–26} temperature, as well as substrate effects,^{27–29} electronic properties,^{30–32} edge configurations,^{33–35} and defects within the graphene structure.^{36–38} The easily detectable Raman bands within graphene include the disordered band at ~1350 cm⁻¹ (D-band), the graphitic band at ~1580 cm⁻¹ (G-band), and a second-order iTO phonon mode at 2630–2700 cm⁻¹ (2D-band). Additionally, an (normally Raman inactive) out-of-plane mode at 867 cm⁻¹,³⁹ several weak combination modes, and second-order overtones do exist⁴⁰ but are usually too weak to be observed in confocal Raman experiments.

Tip-enhanced Raman spectroscopy (TERS) yields the same information as confocal Raman spectroscopy but outperforms it by

* Address correspondence to zenobi@org.chem.ethz.ch.

Received for review September 15, 2011 and accepted September 29, 2011.

Published online 10.1021/nn2035523

© XXXX American Chemical Society

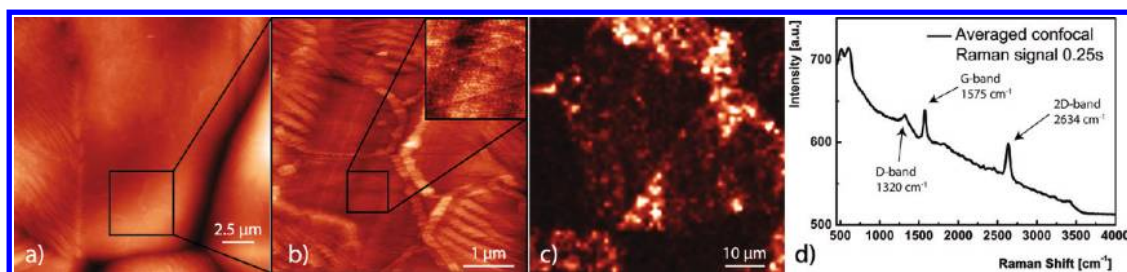


Figure 1. (a,b) STM images from CVD graphene on Cu, 20 μm overview scan and 5 μm zoom showing coarse copper grains and partially folded graphene on top. (c) A 64×64 pixel ($65 \times 65 \mu\text{m}^2$) confocal Raman image (0.25 s/spectrum) from a different area, showing the Raman intensity of the graphene 2D-band. (d) Averaged Raman spectrum from (c) showing only the graphene G- and 2D-band, no CH bending or stretching modes, and only a weak contribution from graphene D-band. In (a,b), brighter color corresponds to an increase in height; in (c), it indicates an increased signal strength of the graphene 2D-band at 2634 cm^{-1} .

far in terms of lateral resolution (increased selectivity) as well as sensitivity (increased signal strength). This is realized by placing a metallic or metal-coated scanning probe microscopy (SPM) tip into the excitation laser focus of a confocal Raman microscope, which confines a part of the laser energy in a very small region underneath the apex of the tip by local enhancement of the electromagnetic (EM) field. With this localized, strong EM field, molecules in a small area are excited, and the resulting enhanced Raman signals report chemical information from this region which is on the order of tens of nanometers. Some TERS experiments on graphene have already been presented in the literature.^{41–44} Hoffmann *et al.* have shown that Raman signals of graphene can be enhanced by TERS; Domke *et al.* showed spectra from graphene as an adlayer on 6H-SiC, and Saito *et al.* showed a TERS image identifying the layer numbers by the signal intensity and correlated it to STM scans. With the exception of the work by Saito, the above only presented point spectra of mixed single and multilayer graphene. Saito *et al.* showed spectral images but only focused on determining the layer number of graphene from the signal loss due to additional graphene layers. Snitka *et al.* added data on the shift of different bands under pressure. None of the above works detected defects or made use of the fact that graphene perpendicular to the excitation direction is only weakly enhanced. Nanoscale detection of defects in carbon-based materials such as carbon nanotubes has been presented before^{45–47} but not on graphene.

In this report, we present a TERS study of graphene on conductive substrates used in research and production. Those suitable for STM distance control, CVD graphene on Cu, and graphene on Au produced by the scotch-tape method were investigated making use of the high spatial resolution, the spectroscopic information, and the selective enhancement in TERS imaging. Bands associated with pristine graphene, hydrogen-terminated graphene, or from contaminations on top of the graphene film, as well as structural defects within the graphene, were assigned and localized with sub-diffraction-limited resolution. The enhancement of the Raman signals allows

TERS to detect very small defects and localized contaminations that would be missed with confocal Raman spectroscopy, which emits less Raman photons. Simultaneously, the graphene bands are only weakly enhanced, allowing detection of the presence of a graphene layer without it interfering with the defect detection. These experiments could help to verify the intended structures of graphene layers produced for electronic devices. By identifying the exact location of defects, electronic properties, such as in single carbon nanoribbons, could be explained, or line defects that are used to increase the conductance along a specific path¹³ could be imaged. High-resolution STM has until now been used to find single atomic mismatches in the graphene lattice, but due to the necessary atomic resolution, the scan sizes usually only cover some tens of nanometers. Using the Raman signature instead of atomic resolution to detect defects, TERS can cover larger areas than STM, on the order of hundreds of nanometers to micrometers, but with additional molecular information compared to the pure structural information in STM. Defects on a scale of tens of nanometers can be detected and localized to within <12 nm.

RESULTS AND DISCUSSION

A sample of graphene produced by CVD, grown on a 20 μm Cu foil, was imaged by STM (Figure 1a,b) and confocal Raman microscopy using $\sim 3 \text{ mW}$, 632.8 nm excitation by a HeNe laser (Figure 1c). The STM image shows the typical large copper grain structures and graphene covering the entire copper substrate with smooth as well as slightly corrugated surface features. The more highly resolved image in (b) shows areas with pristine graphene exhibiting the typical triangular moiré patterns (see inset) similar to observations on Cu and Ni.^{15,16,48} Also, edges and folds of the graphene, which may result from the structure of the underlying copper foil,⁴⁸ are visible. The resolution of the confocal Raman image (c) is around 1 (close to the diffraction limit for this wavelength using a 0.7 NA objective) and was taken from a close-by area. This 64×64 pixel

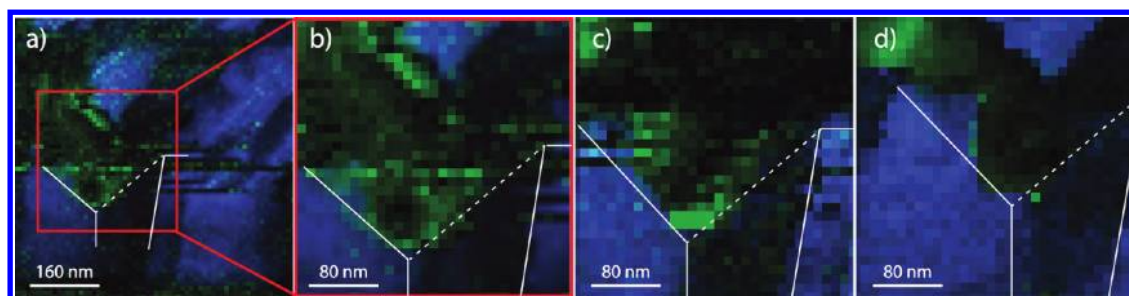


Figure 2. (a) A 64×64 pixel, 640×640 nm² Raman image of graphene on Cu, 0.25 s/spectrum; (b) 32×32 pixel zoom from (a); (c,d) consecutive 32×32 pixel images. (a–d) All images show color-coded band intensities of the graphene 2D-band (green) superimposed on the CH stretching mode (blue). White lines were added to guide the eye. A sample drift of around 20–40 nm toward the top right is visible. Further differences between the measurements could occur due to enhancement fluctuations, noise, or thermally induced changes, which could all affect the displayed band intensities.

image was acquired using a 0.25 s/spectrum integration time. Figure 1d shows an averaged spectrum over the entire confocal image yielding 200 counts per second for the graphene 2D-band at 2634 cm⁻¹. This band can be unambiguously assigned to SLG by its intensity and position under 632.8 nm laser excitation,^{49,50} all indicating the presence of a single layer of graphene on the metal substrate. During this and other confocal scans, no signs of CH bending or stretching modes at the typical positions of 1450 and 2800 – 3000 cm⁻¹, respectively, were detected. Occasionally, very weak signs of defects within the graphene structure were observed, as indicated by the slight shoulder in Figure 1d on the low energy side of the 1570 cm⁻¹ band.

Due to the use of opaque substrates in the production processes of graphene, only a top illumination TERS configuration⁵¹ is suitable to investigate these samples. The same sample as for the confocal experiments was imaged on a scale of 640×640 nm² (the size of a single confocal laser spot), now using TERS imaging (Figure 2). A tip-enhanced Raman spectrum was acquired at every sample location and evaluated for the intensity of certain Raman bands or Raman fingerprint patterns. To ensure sufficient reproducibility of the experiments, the same sample spot in Figure 2 was imaged several times using the same tip, with a step size of 10 nm and 0.25 s/spectrum. Figure 2a shows a 640×640 nm², 64×64 pixel overview image followed by a zoom of the central part and two consecutive 32×32 pixel images of the same area (b–d). Using a short acquisition time, all images were acquired within 35 min, which minimizes but does not eliminate drift. The spectral information content from each Raman image was evaluated and plotted as color-coded intensity maps of the SLG marker bands. The images show the intensity distribution of the graphene 2D-band at 2634 cm⁻¹ in green and the intensity between 2800 and 3000 cm⁻¹, typical for CH stretching modes, in blue. The 32×32 pixel scans clearly show that the measurements are quite reproducible, showing only slight differences and some sample drift. White lines were added to guide the eye. The triangular

blue structures in the upper parts change between the images, and an additional CH-terminated structure appears in Figure 2d, the origin of which we cannot fully explain at present. One possible reason for the changes could be thermally induced changes by the localized field of the tip. An important observation is that the areas covered by pristine graphene and CH-terminated carbon species are clearly anticorrelated. Both signals complement each other well and do not give any indication of graphene-free areas. The coverage agrees with previous reports stating that a continuous film over the entire substrate is produced by the CVD production method.⁹ Yet, no reference to the presence of CH species in these films exists in the literature, most likely because confocal Raman spectroscopy is not sensitive enough to detect them. The weak interactions between graphene and the copper surface allow the graphene film to bridge grain boundaries.⁴⁸ In comparison to the weak confocal Raman signals (with <200 counts per second), the enhanced TERS band intensities range between 4000 and 8000 counts per second for the 2D mode of SLG and 8000–16 000 counts per second for the CH stretching modes, showing the mainly near-field contributions in TERS spectra. The spectroscopic contrast (factor by how much band intensities increase in the presence of the TERS tip)⁵¹ is between 40 and 80 for SLG, while the confocally invisible CH stretching modes are subject to an even higher enhancement, possibly due to their polarizability along the enhanced EM field between tip and surface. An exact value for the enhancement cannot be determined without the far field signal. The lower enhancement for SLG was already observed by Domke *et al.*⁴² and can be explained by the fact that the in-plane vibrational modes of flat graphene are polarized strictly orthogonally to the excitation direction between tip and substrate and the detection direction. Thus, the intensity of the graphene 2D signal is most likely strongly dependent on the structure of the substrate; that is, a higher intensity results when graphene is slightly tilted. Defective graphene areas seem to be less affected by the excitation direction,

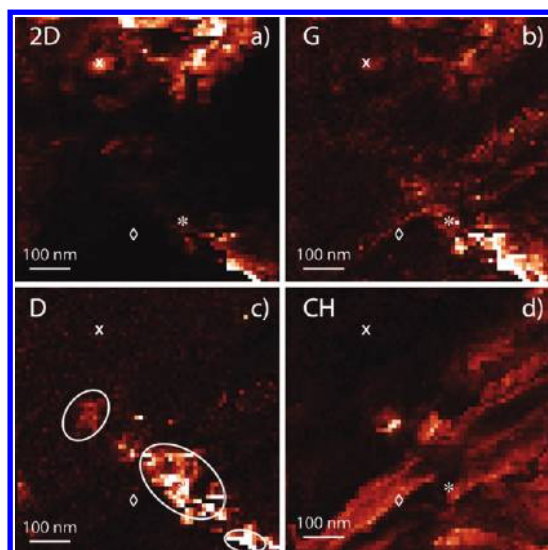


Figure 3. A 64×64 pixel, 640×640 nm² Raman image of graphene on Cu, 0.25 s/spectrum. Background and enhancement corrected band intensity of the (a) 2D-band at 2634 cm⁻¹ typical for single-layer graphene, (b) graphene G-band at 1580 cm⁻¹, (c) D-band at 1350 cm⁻¹, and (d) CH stretching modes at 2800 – 3000 cm⁻¹. Image (c) shows clear localization of graphene defects (white circles) and the complementary behavior of the 2D and CH bands. x, *, and ◇ depict the locations of the spectra shown in Figure 4.

maybe due to broken symmetry. In comparison to the confocal Raman spectrum (Figure 1d) that hardly shows any signs of defects, the TERS spectra (e.g., the red curve in Figure 4) clearly reveal the spectral signature of the D-band and only a small SLG background. This shows that TERS detects these defects far more efficiently than confocal Raman spectroscopy. In confocal RS, the defect covers only a very small portion of the large laser focus surrounded by lots of graphene, in contrast to TERS where a defect can easily be larger than the probed spot size and thus accounts for all of the acquired signal. Thus the relative intensities of defects in graphene appear far smaller in confocal experiments and can easily be lost in the background. To check SLG for the presence of defects, this is quite advantageous as it emphasizes the defects, contaminations, and folds that should be detected, without creating an overwhelming SLG background signal.

A different area on the same sample was imaged with 64×64 pixels, 0.25 s/spectrum on the scale of 640×640 nm²: Figure 3 represents intensities of selected marker bands from within this image, and typical point spectra are shown in Figure 4. Figure 3a–d shows different maps of band intensities within a single Raman image. All spectra for Figure 3 were background-corrected and corrected for enhancement fluctuations by normalization to the local enhancement (using the Raman signals around 130 cm⁻¹ that can be assigned to silver oxide present on the silver tip). The images show the intensity of (a) the 2D-band at 2634 cm⁻¹ typical for SLG, (b) the graphene G-band at 1580 cm⁻¹, (c) the

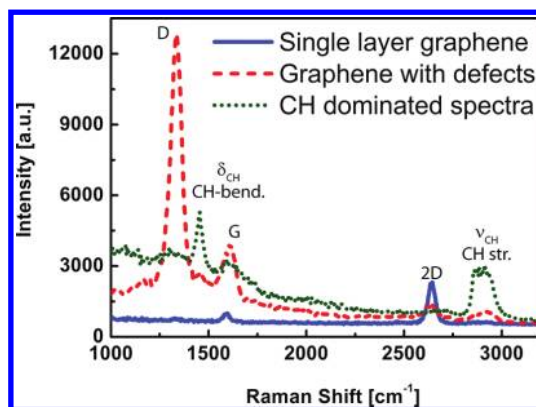


Figure 4. Tip-enhanced Raman spectra of graphene on Cu, 0.25 s, from Figure 3 (indicated by x, *, and ◇) showing typical spectra for single-layer graphene (x, solid blue line), a defect with a pronounced 1350 cm⁻¹ band (*, dashed red line), and a spectrum from an area with contaminated or hydrogen-terminated graphene exhibiting strong CH bending (1450 cm⁻¹) and stretching modes (2800 – 3000 cm⁻¹, ◇, dotted green line).

D-band at 1350 cm⁻¹, and (d) the CH stretching mode at 2800 – 3000 cm⁻¹.

In the upper left part, an area of pristine SLG dominates all of the spectra, showing neither defects nor CH contamination or edges (Figure 4, solid blue line). In the bottom right half of the image, two areas can be distinguished. The diagonal feature reaching from the middle toward the edge of the frame exhibits signals from D-, G-, and the 2D-band, which leads to the conclusion that this is a single layer of graphene with either weak defects or contamination (Figure 4, dashed red line). The areas left and right of this diagonal feature show some G-band and mainly CH stretching and CH bending mode intensity (Figure 4, dotted green line). This leads to the conclusion that this area contains hydrogen-terminated carbon atoms from either a graphene edge region or an organic contaminant. A contaminant, however, should still exhibit SLG signals to some extent, and the edge region should be considerably smaller. A third possibility is thus the presence of partly H-terminated graphene, which is left over from the production process.

The detected defects in Figure 3c highlighted by white circles are restricted to areas only 100×150 nm², 100×250 nm², and 50×100 nm² in size. This underscores that we can benefit from the high resolution of TERS to determine the exact size and position of defects. Moreover, due to the strong enhancement, it is possible to detect these small, weakly scattering defects.

From a thin uniform graphene film, one would intuitively expect a constant Raman signal over the entire measurement. Yet, as discussed above, several effects in a TERS measurement can be superimposed on the constant signal. First, small fluctuations in the feedback change the local EM field strength and thus the Raman intensity. Even more importantly, surface

corrugations of the substrate, as well as slight changes in the orientation of the graphene lead to a better overlap of the EM field used for excitation with the polarizability of the graphene modes. Although excited by a focused Gaussian beam, a considerable amount of polarization of the EM field along the direction of the tip axis can be expected in gap mode,^{52–54} which does not efficiently overlap with the in-plane Raman modes of the graphene. Depending on the angle and thus the overlap, the detected local intensity of certain SLG flakes changes dramatically (compare Figure 5).

We also investigated samples produced by the second widely used production method, the scotch-tape method. A graphene sample was prepared according to standard protocols² and deposited on template-stripped gold. TERS imaging was performed on sample areas preselected in an optical microscope containing thin graphene flakes. Figure 5 shows a 100×100 pixel, $400 \times 400 \text{ nm}^2$ TERS image taken in a preselected area. The green color again represents the intensity of the 2D-band from SLG, while the red color shows the D-band intensity typical for sample defects. Within the image, a small, very intense SLG area can be found (white dashed circle, and Figure 5b, green spectrum). The surrounding area still exhibits SLG signals, albeit far weaker (by a factor of ≈ 20). Due to the high contrast, these signals are hardly visible in this two-colored representation. Two defects within the surrounding graphene layer were identified due to their spectroscopic signature depicted in Figure 5b (red spectrum) and marked with white circles. The dimensions of these defects are $75 \times 45 \text{ nm}^2$ and $55 \times 25 \text{ nm}^2$, respectively. The spatial resolution of the Raman map was determined at two separate locations in the image, indicated by white dotted lines. The fwhm of these curves was determined by fitting the line profiles of the 2D- and the D-band with a Gaussian to be 10.6 and 11.8 nm fwhm, respectively. The spectra collected in the upper and the right part of the image exhibit a different shape and intensity and do not show the 2D-band of SLG. This indicates a graphene free region with signals from amorphous carbonaceous material (black spectrum in Figure 5b).

CONCLUSIONS

An investigation of graphene, based on the TERS spectroscopic signatures of pristine, defective, and contaminated/H-terminated graphene, has been presented with a resolution of $<12 \text{ nm}$. The expected single-layer thickness was confirmed from the position of the 2D Raman band. The dependence of the Raman enhancement on the orientation of graphene was found to reduce the signal intensity from graphene itself, allowing to easily localize defects, folds, and contamination signals on a moderate SLG signal background. Confocal Raman spectroscopy, in contrast, has 1–2

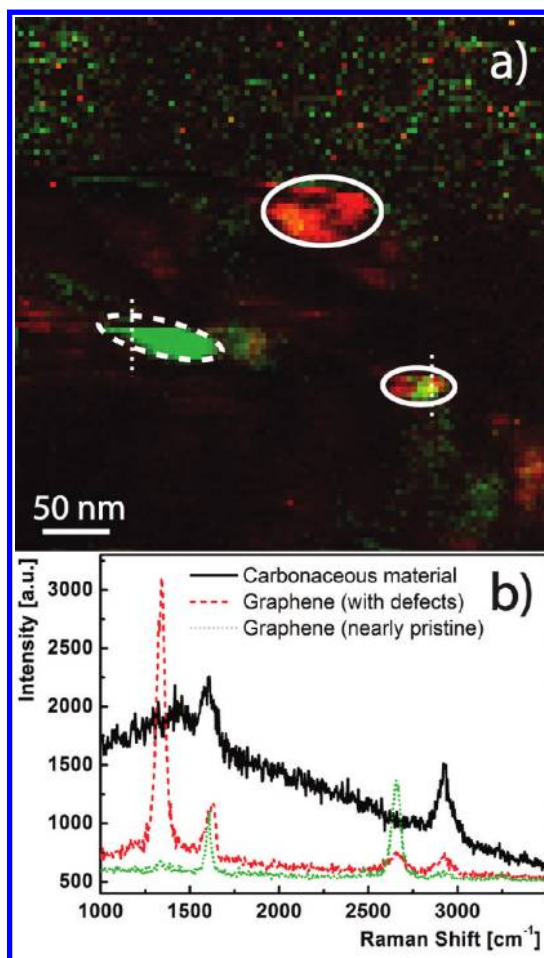


Figure 5. (a) A 100×100 pixel, $400 \times 400 \text{ nm}^2$ Raman image of graphene on template-stripped gold, produced by the scotch-tape technique, 0.3 s/pixel . Band intensity of 2D-band at $<2662 \text{ cm}^{-1}$ (green) typical for SLG superimposed with intensity of graphene D-band at 1350 cm^{-1} . Areas with strong defects are visible (white circles, $75 \times 45 \text{ nm}^2$ and $55 \times 25 \text{ nm}^2$) as well as a small area with intense graphene signals (dashed white line). The weaker graphene signals in most of the background are not visible due to the enormous contrast. (b) Characteristic Raman spectra from the SLG (green), one defect area (red), and the graphene free background (black). Resolution has been determined by a Gauss fit on the white dotted lines as 10.6 and 11.8 nm fwhm, respectively.

orders of magnitude poorer spatial resolution and exhibits identical intensity for flat and corrugated areas. It thus often neglects small defects or folds within large pristine graphene areas. Small defects inside continuous single-layer graphene films were identified with TERS and localized with high precision. The high signal-to-noise ratio in the spectra (due to the contrast factor of up to >80 with respect to confocal Raman microscopy) implies that, by using TERS, even smaller defects at the resolution limit on the order of $10\text{--}15 \text{ nm}$ can be localized. This detection and localization of small defects will be crucial for the production of reliable electronic structures and devices due to their influence on the electronic properties of graphene structures (e.g., nanoribbons). The presented

measurements were conducted on two different samples based on gold as well as copper, produced with standard commercial graphene production methods in use. They promise a potential use of

tip-enhanced Raman spectroscopic imaging to control the quality of graphene layers on a wide variety of substrates before or after transfer onto Si for use in molecular electronics.

MATERIALS AND METHODS

Samples of graphene on gold were produced by coating >50 nm of gold onto silicon wafers, followed by a template stripping process similar to the one described by Hegner *et al.*⁵⁵ Freshly cleaved graphite was rubbed against the exposed gold surface to transfer graphene, and excess graphite was removed by the scotch-tape method.² Samples of graphene on copper consisted of commercially available SLG on a 20 μm copper foil (Graphene Laboratories Inc., Ronkonkoma, USA) produced by CVD.⁹

Silver tips for the TERS experiments (99.99% Ag wire, 0.25 mm, Aldrich) were etched similar to previous reports^{56,57} in a solution of 1:1 to 1:2 (v/v) of perchloric acid (Riedel de Haen)/methanol, with an etching voltage of 8 V, and preselected using a 360 \times stereomicroscope (Nikon, Amstelveen, The Netherlands).

Raman spectra were collected on a combined AFM/STM instrument connected to a quadruple grating Raman spectrometer (NTMDT Ntegra Spectra, Zelenograd, Russia) equipped with an EMCCD (iDus 720, Andor Newton, Belfast, UK). The tip-enhanced Raman data were acquired using top-illumination and top-collection as described in detail by Stadler *et al.*⁵¹

For each TERS experiment, the laser (632.8 nm helium–neon) was carefully focused and locked onto the approached STM tip and the sample scanned underneath both. The laser power at the sample was usually between 0.1 and 2 mW, and a collection time between 0.1 and 1 s per spectrum was used.

The acquired 4D TERS imaging data (x , y , Raman shift, intensity) was processed directly in the proprietary instrument software and exported as images or ASCII data. No background corrections were made for the spectra shown except for the mentioned changes in Figure 3. For the Raman images, band intensities with respect to the surrounding background were determined and color-coded. A linear slope correction was applied for the STM images to correct for sample drift in the z -direction.

REFERENCES AND NOTES

- Kroto, H. W.; Heath, J. R.; O'Brien, S. C.; Curl, R. F.; Smalley, R. E. C60: Buckminsterfullerene. *Nature* **1985**, *318*, 162–163.
- Novoselov, K. S.; Geim, A. K.; Morozov, S. V.; Jiang, D.; Zhang, Y.; Dubonos, S. V.; Grigorieva, I. V.; Firsov, A. A. Electric Field Effect in Atomically Thin Carbon Films. *Science* **2004**, *306*, 666–669.
- Novoselov, K. S.; Jiang, D.; Schedin, F.; Booth, T. J.; Khotkevich, V. V.; Morozov, S. V.; Geim, A. K. Two-Dimensional Atomic Crystals. *Proc. Natl. Acad. Sci. U.S.A.* **2005**, *102*, 10451–10453.
- Chen, J. H.; Ishigami, M.; Jang, C.; Hines, D. R.; Fuhrer, M. S.; Williams, E. D. Printed Graphene Circuits. *Adv. Mater.* **2007**, *19*, 3623–3627.
- Schwierz, F. Graphene Transistors. *Nat. Nanotechnol.* **2010**, *5*, 487–496.
- Lin, Y.-M.; Jenkins, K. A.; Valdes-Garcia, A.; Small, J. P.; Farmer, D. B.; Avouris, P. Operation of Graphene Transistors at Gigahertz Frequencies. *Nano Lett.* **2008**, *9*, 422–426.
- Yoo, J. J.; Balakrishnan, K.; Huang, J. S.; Meunier, V.; Sumpter, B. G.; Srivastava, A.; Conway, M.; Reddy, A. L. M.; Yu, J.; Vajtai, R.; Ajayan, P. M. Ultrathin Planar Graphene Supercapacitors. *Nano Lett.* **2011**, *11*, 1423–1427.
- Xia, F.; Mueller, T.; Lin, Y.-m.; Valdes-Garcia, A.; Avouris, P. Ultrafast Graphene Photodetector. *Nat. Nanotechnol.* **2009**, *4*, 839–843.
- Li, X.; Cai, W.; An, J.; Kim, S.; Nah, J.; Yang, D.; Piner, R.; Velamakanni, A.; Jung, I.; Tutuc, E.; Banerjee, S. K.; Colombo, L.; Ruoff, R. S. Large-Area Synthesis of High-Quality and Uniform Graphene Films on Copper Foils. *Science* **2009**, *324*, 1312–1314.
- Li, X.; Zhu, Y.; Cai, W.; Borysiak, M.; Han, B.; Chen, D.; Piner, R. D.; Colombo, L.; Ruoff, R. S. Transfer of Large-Area Graphene Films for High-Performance Transparent Conductive Electrodes. *Nano Lett.* **2009**, *9*, 4359–4363.
- Gallagher, P.; Todd, K.; Goldhaber-Gordon, D. Disorder-Induced Gap Behavior in Graphene Nanoribbons. *Phys. Rev. B: Condens. Matter Mater. Phys.* **2010**, *81*, 115409.
- Banhart, F.; Kotakoski, J.; Krasheninnikov, A. V. Structural Defects in Graphene. *ACS Nano* **2011**, *5*, 26–41.
- Botello-Mendez, A. R.; Lopez-Urias, F.; Cruz-Silva, E.; Sumpter, B. G.; Meunier, V.; Terrones, M.; Terrones, H. The Importance of Defects for Carbon Nanoribbon Based Electronics. *Phys. Status Solidi RRL* **2009**, *3*, 181–183.
- Schaeffel, F.; Wilson, M.; Bachmatiuk, A.; Ruemmel, M. H.; Queitsch, U.; Rellinghaus, B.; Briggs, G. A. D.; Warner, J. H. Atomic Resolution Imaging of the Edges of Catalytically Etched Suspended Few-Layer Graphene. *ACS Nano* **2011**, *5*, 1975–1983.
- Zhao, R.; Zhang, Y.; Gao, T.; Gao, Y.; Liu, N.; Fu, L.; Liu, Z. Scanning Tunneling Microscope Observations of Non-AB Stacking of Graphene on Ni Films. *Nano Res.* **2011**, *1*–10.
- Zhang, Y.; Gao, T.; Gao, Y.; Xie, S.; Ji, Q.; Yan, K.; Peng, H.; Liu, Z. Defect-like Structures of Graphene on Copper Foils for Strain Relief Investigated by High-Resolution Scanning Tunneling Microscopy. *ACS Nano* **2011**, *5*, 4014–4022.
- Wang, H.; Wang, Y.; Cao, X.; Feng, M.; Lan, G. Vibrational Properties of Graphene and Graphene Layers. *J. Raman Spectrosc.* **2009**, *40*, 1791–1796.
- Tommasini, M.; Castiglioni, C.; Zerbi, G. Raman Scattering of Molecular Graphenes. *Phys. Chem. Chem. Phys.* **2009**, *11*, 10185–10194.
- Connolly, M. R.; Smith, C. G. Nanoanalysis of Graphene Layers Using Scanning Probe Techniques. *Philos. Trans. R. Soc., A* **2010**, *368*, 5379–5389.
- Ni, Z. H.; Wang, Y. Y.; Yu, T.; Shen, Z. X. Raman Spectroscopy and Imaging of Graphene. *Nano Res.* **2008**, *1*, 273–291.
- Dresselhaus, M. S.; Dresselhaus, G.; Hofmann, M. Raman Spectroscopy as a Probe of Graphene and Carbon Nanotubes. *Philos. Trans. R. Soc., A* **2008**, *366*, 231–236.
- Hao, Y. F.; Wang, Y. Y.; Wang, L.; Ni, Z. H.; Wang, Z. Q.; Wang, R.; Koo, C. K.; Shen, Z. X.; Thong, J. T. L. Probing Layer Number and Stacking Order of Few-Layer Graphene by Raman Spectroscopy. *Small* **2010**, *6*, 195–200.
- Yoon, D.; Moon, H.; Cheong, H.; Choi, J. S.; Choi, J. A.; Park, B. H. Variations in the Raman Spectrum as a Function of the Number of Graphene Layers. *J. Korean Phys. Soc.* **2009**, *55*, 1299–1303.
- Yu, T.; Ni, Z. H.; Du, C. L.; You, Y. M.; Wang, Y. Y.; Shen, Z. X. Raman Mapping Investigation of Graphene on Transparent Flexible Substrate: The Strain Effect. *J. Phys. Chem. C* **2008**, *112*, 12602–12605.
- Young, R. J.; Gong, L.; Kinloch, I. A.; Riaz, I.; Jalil, R.; Novoselov, K. S. Strain Mapping in a Graphene Monolayer Nanocomposite. *ACS Nano* **2011**, *5*, 3079–3084.
- Huang, M.; Yan, H.; Chen, C.; Song, D.; Heinz, T. F.; Hone, J. Phonon Softening and Crystallographic Orientation of Strained Graphene Studied by Raman Spectroscopy. *Proc. Natl. Acad. Sci. U.S.A.* **2009**, *106*, 7304–7308.
- Zhou, H. Q.; Qiu, C. Y.; Yu, F.; Yang, H. C.; Chen, M. J.; Hu, L. J.; Guo, Y. J.; Sun, L. F. Raman Scattering of Monolayer Graphene: The Temperature and Oxygen Doping Effects. *J. Phys. D: Appl. Phys.* **2011**, *44*, 185404.

28. Calizo, I.; Ghosh, S.; Bao, W. Z.; Miao, F.; Lau, C. N.; Balandin, A. A. Raman Nanometrology of Graphene: Temperature and Substrate Effects. *Solid State Commun.* **2009**, *149*, 1132–1135.
29. Wang, Y. Y.; Ni, Z. H.; Yu, T.; Shen, Z. X.; Wang, H. M.; Wu, Y. H.; Chen, W.; Wee, A. T. S. Raman Studies of Monolayer Graphene: The Substrate Effect. *J. Phys. Chem. C* **2008**, *112*, 10637–10640.
30. Molitor, F.; Graf, D.; Stampfer, C.; Ihn, T.; Ensslin, K. In *Advances in Solid State Physics*; Haug, R., Ed.; Springer: Berlin/Heidelberg, 2008; Vol. 47, pp 171–176.
31. Malard, L. M.; Mafra, D. L.; Doorn, S. K.; Pimenta, M. A. Resonance Raman Scattering in Graphene: Probing Phonons and Electrons. *Solid State Commun.* **2009**, *149*, 1136–1139.
32. Wang, R.; Wang, S.; Zhang, D.; Li, Z.; Fang, Y.; Qiu, X. Control of Carrier Type and Density in Exfoliated Graphene by Interface Engineering. *ACS Nano* **2011**, *5*, 408–412.
33. Gupta, A. K.; Russin, T. J.; Gutierrez, H. R.; Eklund, P. C. Probing Graphene Edges via Raman Scattering. *ACS Nano* **2009**, *3*, 45–52.
34. Cong, C.; Yu, T.; Wang, H. Raman Study on the G Mode of Graphene for Determination of Edge Orientation. *ACS Nano* **2010**, *4*, 3175–3180.
35. Jia, X.; Campos-Delgado, J.; Terrones, M.; Meunier, V.; Dresselhaus, M. S. Graphene Edges: A Review of Their Fabrication and Characterization. *Nanoscale* **2011**, *3*, 86–95.
36. Das, A.; Chakraborty, B.; Sood, A. K. Raman Spectroscopy of Graphene on Different Substrates and Influence of Defects. *Bull. Mater. Sci.* **2008**, *31*, 579–584.
37. Heydrich, S.; Hirmer, M.; Preis, C.; Korn, T.; Eroms, J.; Weiss, D.; Schuller, C. Scanning Raman Spectroscopy of Graphene Antidot Lattices: Evidence for Systematic p-Type Doping. *Appl. Phys. Lett.* **2010**, *97*, 043113.
38. Dresselhaus, M. S.; Jorio, A.; Souza Filho, A. G.; Saito, R. Defect Characterization in Graphene and Carbon Nanotubes Using Raman Spectroscopy. *Philos. Trans. R. Soc., A* **2010**, *368*, 5355–5377.
39. Kawashima, Y.; Katagiri, G. Observation of the Out-of-Plane Mode in the Raman Scattering From the Graphite Edge Plane. *Phys. Rev. B: Condens. Matter Mater. Phys.* **1999**, *59*, 62.
40. Cong, C.; Yu, T.; Saito, R.; Dresselhaus, G. F.; Dresselhaus, M. S. Second-Order Overtone and Combination Raman Modes of Graphene Layers in the Range of 1690–2150 cm^{-1} . *ACS Nano* **2011**, *5*, 1600–1605.
41. Hoffmann, G. G.; de With, G.; Loos, J. Micro-Raman and Tip-Enhanced Raman Spectroscopy of Carbon Allotropes. *Macromol. Symp.* **2008**, *265*, 1–11.
42. Domke, K. F.; Pettinger, B. Tip-Enhanced Raman Spectroscopy of 6H-SiC with Graphene Adlayers: Selective Suppression of E1 Modes. *J. Raman Spectrosc.* **2009**, *40*, 1427–1433.
43. Saito, Y.; Verma, P.; Masui, K.; Inouye, Y.; Kawata, S. Nano-scale Analysis of Graphene Layers by Tip-Enhanced Near-Field Raman Spectroscopy. *J. Raman Spectrosc.* **2009**, *40*, 1434–1440.
44. Snitka, V.; Rodrigues, R. D.; Lendraitis, V. Novel Gold Cantilever for Nano-Raman Spectroscopy of Graphene. *Microelectron. Eng.* **2011**, *88*, 2759–2762.
45. Maciel, I. O.; Anderson, N.; Pimenta, M. A.; Hartschuh, A.; Qian, H.; Terrones, M.; Terrones, H.; Campos-Delgado, J.; Rao, A. M.; Novotny, L.; Jorio, A. Electron and Phonon Renormalization near Charged Defects in Carbon Nanotubes. *Nat. Mater.* **2008**, *7*, 878–883.
46. Georgi, C.; Hartschuh, A. Tip-Enhanced Raman Spectroscopic Imaging of Localized Defects in Carbon Nanotubes. *Appl. Phys. Lett.* **2010**, *97*, 143117.
47. Chan, K. L. A.; Kazarian, S. G. Finding a Needle in a Chemical Haystack: Tip-Enhanced Raman Scattering for Studying Carbon Nanotubes Mixtures. *Nanotechnology* **2010**, *21*.
48. Cho, J.; Gao, L.; Tian, J.; Cao, H.; Wu, W.; Yu, Q.; Yitamben, E. N.; Fisher, B.; Guest, J. R.; Chen, Y. P.; Guisinger, N. P. Atomic-Scale Investigation of Graphene Grown on Cu Foil and the Effects of Thermal Annealing. *ACS Nano* **2011**, *5*, 3607–3613.
49. Ferrari, A. C.; Meyer, J. C.; Scardaci, V.; Casiraghi, C.; Lazzeri, M.; Mauri, F.; Piscanec, S.; Jiang, D.; Novoselov, K. S.; Roth, S.; Geim, A. K. Raman Spectrum of Graphene and Graphene Layers. *Phys. Rev. Lett.* **2006**, *97*, 187401.
50. Park, J. S.; Reina, A.; Saito, R.; Kong, J.; Dresselhaus, G.; Dresselhaus, M. S. G' Band Raman Spectra of Single, Double and Triple Layer Graphene. *Carbon* **2009**, *47*, 1303–1310.
51. Stadler, J.; Schmid, T.; Zenobi, R. Nanoscale Chemical Imaging Using Top-Illumination Tip-Enhanced Raman Spectroscopy. *Nano Lett.* **2010**, *10*, 4514–4520.
52. Demming, A. L.; Festy, F.; Richards, D. Plasmon Resonances on Metal Tips: Understanding Tip-Enhanced Raman Scattering. *J. Chem. Phys.* **2005**, *122*, 184716.
53. Foteinopoulou, S.; Vigneron, J. P.; Vandenbem, C. Optical Near-Field Excitations on Plasmonic Nanoparticle-Based Structures. *Opt. Express* **2007**, *15*, 4253–4267.
54. Picardi, G.; Chaigneau, M.; Ossikovski, R.; Licitra, C.; Delapierre, G. Tip Enhanced Raman Spectroscopy on Azobenzene Thiol Self-Assembled Monolayers on Au(111). *J. Raman Spectrosc.* **2009**, *40*, 1407–1412.
55. Hegner, M.; Wagner, P.; Semenza, G. Ultralarge Atomically Flat Template-Stripped Au Surfaces for Scanning Probe Microscopy. *Surf. Sci.* **1993**, *291*, 39–46.
56. Ibe, J. P.; P. P. Bey, J.; Brandow, S. L.; Brizzolara, R. A.; Burnham, N. A.; DiLella, D. P.; Lee, K. P.; Marrian, C. R. K.; Colton, R. J. On the Electrochemical Etching of Tips for Scanning Tunneling Microscopy. *J. Vac. Sci. Technol., A* **1990**, *8*, 3570–3575.
57. Zhang, W. H.; Cui, X. D.; Yeo, B. S.; Schmid, T.; Hafner, C.; Zenobi, R. Nanoscale Roughness on Metal Surfaces Can Increase Tip-Enhanced Raman Scattering by an Order of Magnitude. *Nano Lett.* **2007**, *7*, 1401–1405.